REPORT DOCUMENTATION PAGE

AFRL-SR-BL-TR-98-0254

1. AGENCY USE ONLY (Leave blank)	2. REPORT DATE	3. REPORT TYPE AND DATES COVERED
	March 17, 1998	Final Report (4/1/95-9/30/97)

4. TITLE AND SUBTITLE
Electron Transport in Coupled Quantum Dots

5. FUNDING NUMBERS
C F49620-95-1-0311

6. AUTHOR(S)
D. A. Antoniadis, H. I. Smith, and T. P. Orlando

7. PERFORMING ORGANIZATION NAME(S) AND ADDRESS(ES)
Department of Electrical Engineering and Computer Science
Massachusetts Institute of Technology
60 Vassar Street, Cambridge, MA 02139

8. PERFORMING ORGANIZATION REPORT NUMBER

9. SPONSORING/MONITORING AGENCY NAME(S) AND ADDRESS(ES)
AFOSR/NE
110 Duncan Avenue, Suite B115
Bolling AFB, DC 20332

10. SPONSORING/MONITORING AGENCY REPORT NUMBER

11. SUPPLEMENTARY NOTES

12a. DISTRIBUTION/AVAILABILITY STATEMENT
Unlimited

19980331 032

13. ABSTRACT (Maximum 200 words)

In the course of the investigation funded by this proposal we fabricated, modeled, and measured a variety of quantum dot structures in order to better understand how such nanostructures might be used for computation. Our interest in doing so was motivated by discussions in the literature of radically different schemes for computation involving cellular-automata or quantum-mechanical computation. Understanding how quantum dots interact with each other and with their leads is important to their potential application in these schemes.

14. SUBJECT TERMS	15. NUMBER OF PAGES 16
	16. PRICE CODE

17. SECURITY CLASSIFICATION OF REPORT	18. SECURITY CLASSIFICATION OF THIS PAGE	19. SECURITY CLASSIFICATION OF ABSTRACT	20. LIMITATION OF ABSTRACT

Final Report for
Electron Transport in Coupled Quantum Dots
F49620-95-1-0311

D. A. Antoniadis, H. I. Smith and T. P. Orlando
Department of Electrical Engineering and Computer Science
Massachusetts Institute of Technology

March 17, 1998

Contents

1 Executive Summary **1**

2 Coupled Quantum Dot Structures **2**

3 Numerical Simulations **7**

4 Arrays of Quantum Dots **11**
4.1 One-dimensional arrays 11
4.2 Two-dimensional arrays 14

5 Publications and Talks **15**
5.1 Papers 15
5.2 Talks 15

1 Executive Summary

In the course of the investigation funded by this proposal we fabricated, modeled, and measured a variety of quantum dot structures in order to better understand how such nanostructures might be used for computation. Our interest in doing so was motivated by discussions in the literature of radically different schemes for computation involving cellular-automata or quantum-mechanical computation [1–4]. Understanding how quantum dots interact with each other and with their leads is important to their potential application in these schemes.

Our work has focused on the following three main areas:

1. **Coupled Quantum Dot Structures:** We fabricated coupled dot structures by both electron-beam (e-beam) and x-ray nanolithography. Our work in this area focused around a unique coupled quantum dot structure which provides coupling not through a quantum point contact (QPC) but through a tunnel barrier formed by a narrow gate. This narrow gate device should show significantly different behavior from other quantum dot systems coupled via QPC's reported in the literature. Because our e-beam tools were unable to reliably fabricate

device structures below about 60 nm in dimension, it was decided to use x-ray lithography to fabricate the structures.

In fabricating these extremely fine lines, we pushed the x-ray nanolithography device fabrication process further than it had been previously pushed and discovered an effect due to photoelectron generation in the substrate which was limiting our mask resolution. A modification of our process allowed us to fabricate the necessary masks and devices, and ultimately will allow for greater process latitude for devices which have features in the sub-50 nm regime. This work has led to one published paper.

2. **Numerical Simulations of Devices:** We developed software tools to simulate electron transport through single- and multiple-quantum-dot structures. These tools were the first to include the full capacitance matrix in the transport characteristics. We used these tools to investigate the static and dynamical properties of quantum dot arrays and single dots with superconducting leads. This work also led to the study of the nature of the statistical distribution of energy-level spacings in two-dimensional harmonic oscillators. Our simultation work has resulted in three published papers and three conference presentations.

3. **Arrays of Quantum Dots:** We fabricated a one-dimensional array of seven quantum dots using direct-write e-beam lithography. The devices have been used in double-dot experiments with varying inter-dot coupling. Two-dimensional arrays of quantum dots were also fabricated.

2 Coupled Quantum Dot Structures

Of particular interest to the research community, and for the prospects of computation with Coulomb blockade structures, is how the transport properties of individual or coupled quantum dot structures change as the dot goes from being weakly coupled to its environment and (therefore having a well-defined charge) to being strongly coupled to its environment (therefore not having a well-defined charge).

Previous experiments [5] in semiconductor nanostructures have focused on quantum dots coupled to their environment or to each other via quantum point contacts (QPC's). As these QPC's are opened to allow the dot to couple to its electronic environment, a single electron transport channel opens. When one transport channel is opened fully (such that its transmission probability is equal to unity), the quantum dot no longer has a well-defined charge state and Coulomb blockade effects disappear.

We fabricated a different type of quantum dot structure in which the transition from weak environmental coupling to strong coupling happens not through the opening of one channel, but through the opening of many channels with small transmission probabilities. This is done by using a fine-line gate to form a tunnel barrier between dots. In this case the physics of the transport should be much more like that of a metal tunnel barrier, such as those used in Josephson junctions or metal coulomb-blockade devices. Figure 1 shows the two types of double-dot structures, one with a fine-line tunnel barrier between the dots and one with a QPC between them. By fabricating both devices on the same chip, a number of experiments could be done comparing the behavior of the two barrier types in single and double-dot configurations.

To fabricate the tunnel barrier structure in such a way as to have good control over the strength of the barrier with an external voltage source, it is necessary to have extremely fine lines. In order to push these widths as low as possible, it was decided to use x-ray nanolithography, which has no

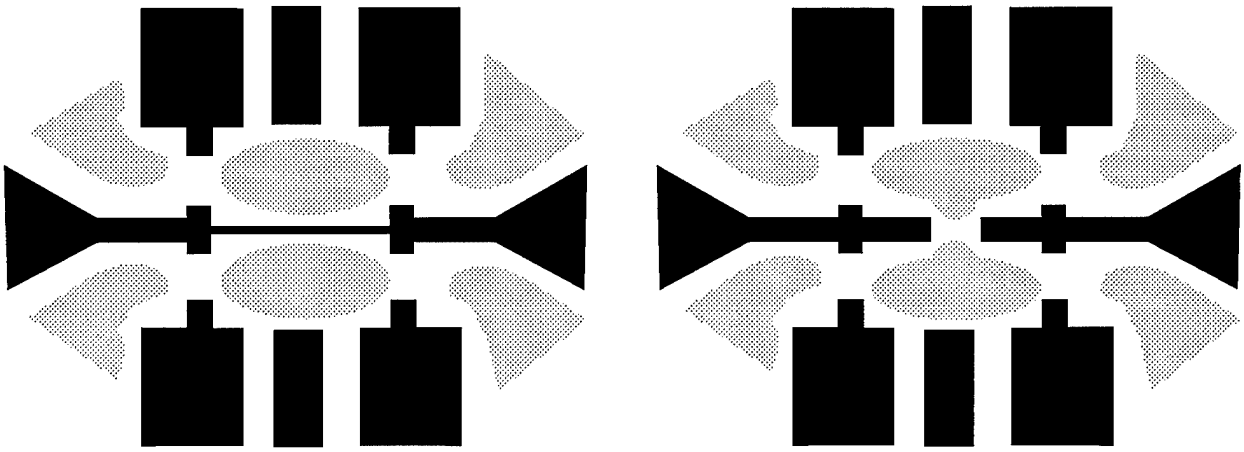

Figure 1: Schematic view of two coupled quantum dot devices. Black areas indicate Schottky gates on the GaAs heterostructure. Shaded areas indicate regions where the two-dimensional electron gas is not depleted. In device a) the dots are coupled via a tunnel barrier formed by a fine-line gate. In device b) the dots are coupled via a quantum point contact.

line-widening effects due to backscattered electrons from the semiconductor substrate as is found in an electron-beam direct write process. (Because of these effects, our e-beam tools were incapable of reliably writing sub-60 nm lines on a substrate). In choosing to use x-ray nanolithography for fabrication, we were pushing the full x-ray fabrication process further than it had been pushed before.

Even though the fine-line tunnel barrier structure was not able to be written by e-beam lithography, gate structures on devices coupled by QPCs were successfully fabricated. Figure 2 shows an SEM micrograph of Ti/Au gates on a GaAs substrate.

X-ray "mother" masks with the novel coupled quantum dot design were designed by us and written at the Naval Research Laboratory. These masks were processed in our laboratory and had linewidths down to ~30 nm. An AFM micrograph of a device structure on the mother mask is shown in Figure 3.

To print a device from this mask, a negative replica or a "daughter" mask had to be made. In the fabrication of this "daughter" mask, the "mother" mask is used to expose a PMMA mold into which gold is electroplated. The fine gold line on the mother becomes a PMMA line on the daughter with approximately the same width, 200 nm height, and ~1 μm length. We had problems in our many attempts to create this daughter; the fine line of PMMA would lose adherence during the development and plating processes.

We were finally able to track the adhesion problems to a substrate photoelectron effect – x-rays which are absorbed strongly in the gold plating base on the daughter mask generate photoelectrons which make their way into the bottom layer of the PMMA and create additional exposure. This effect apparently has a lateral range of approximately 20 nm which is enough to undercut a 40 nm line and prevent it from adhering. The effect had not been seen before because lines wider than 40 nm on daughter masks were able to adhere and the plated mask and devices printed from it looked fine. It was only in pushing the full device fabrication process with x-ray nanolithography

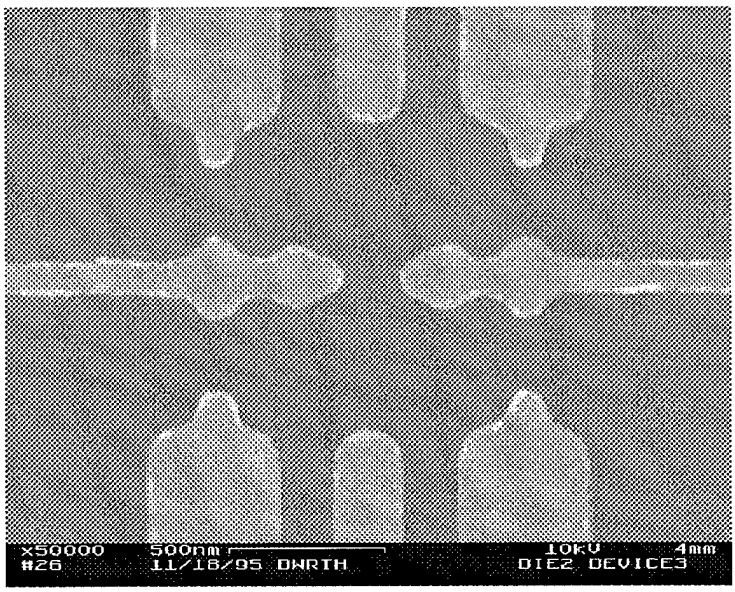

Figure 2: SEM micrograph of an electron-beam direct-written coupled quantum dot device on a GaAs/AlGaAs heterostructure.

that the impact of this substrate photoelectron effect was revealed.

Once the effect was understood a way around it was found – use a thinner gold plating base (approximately one monolayer) to minimize the generation of photoleletrons. By absorbing fewer x-rays in the plating base, less excess dose is given to the resist interface layer. An SEM micrograph of a device on a daughter mask is shown in Figure 4. Note the 20 nm linewidth of the gap in the gold (which had been a PMMA space).

Devices were fabricated using this "daughter" mask. SEM micrographs of the complete sequence of "mother" mask, "daughter" mask, and device are shown in Figure 5.

Further experiments are underway to better understand and control the substrate photoelectron effect and to determine the ultimate resolution limits of x-ray nanolithography, and to characterize process latitude at these ultra-small feature sizes.

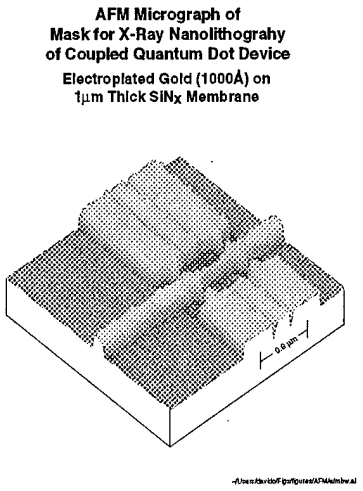

Figure 3: AFM micrograph of an x-ray mask for a double-dot structure. The image is of thick ($\sim$1000) gold on a 1 μm-thick SiN_x membrane.

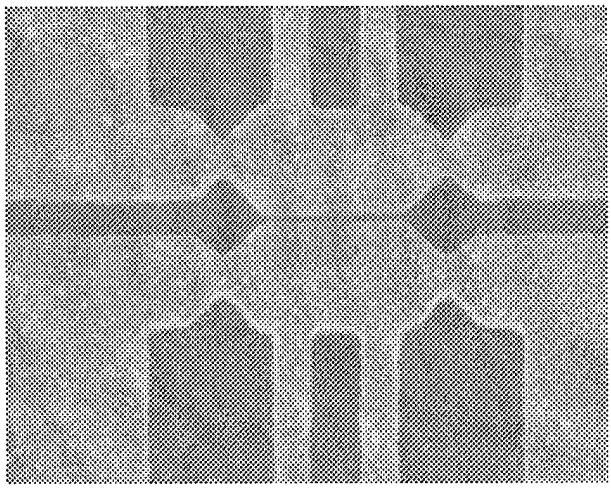

Figure 4: SEM micrograph of a coupled quantum dot gate pattern on a "daughter" mask. The fine line is only 20 nm wide, indicating the substrate photoelectrons did not compromise PMMA adhesion.

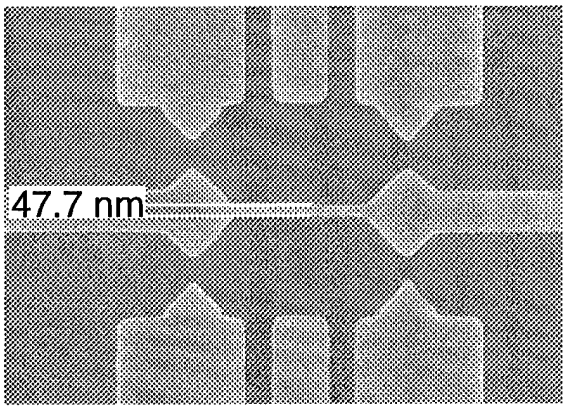

a)"Mother" Mask
(Au on SiNx membrane)

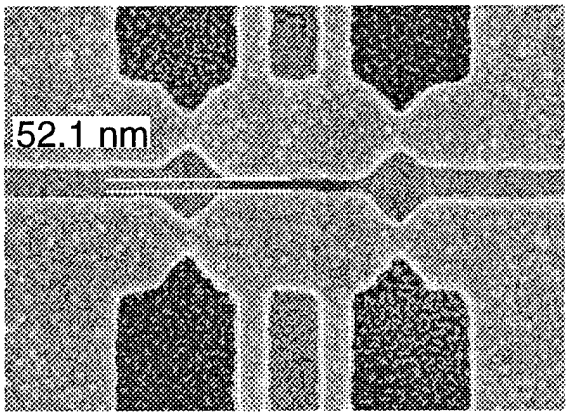

b)"Daughter" Mask
(Au on SiNx membrane)

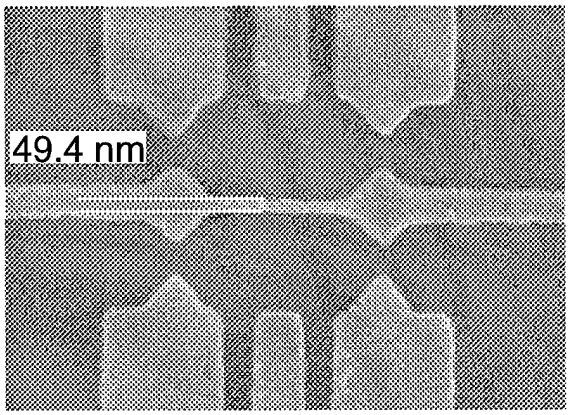

c) Quantum Dot Device
(AuPd on GaAs)

Figure 5: SEM micrographs of a coupled quantum dot device on (a) a "mother" mask, (b) a "daughter" mask, and (c) the Schottky gates on top of a GaAs/AlGaAs heterostructure. The width of the fine line middle gate is noted in each micrograph.

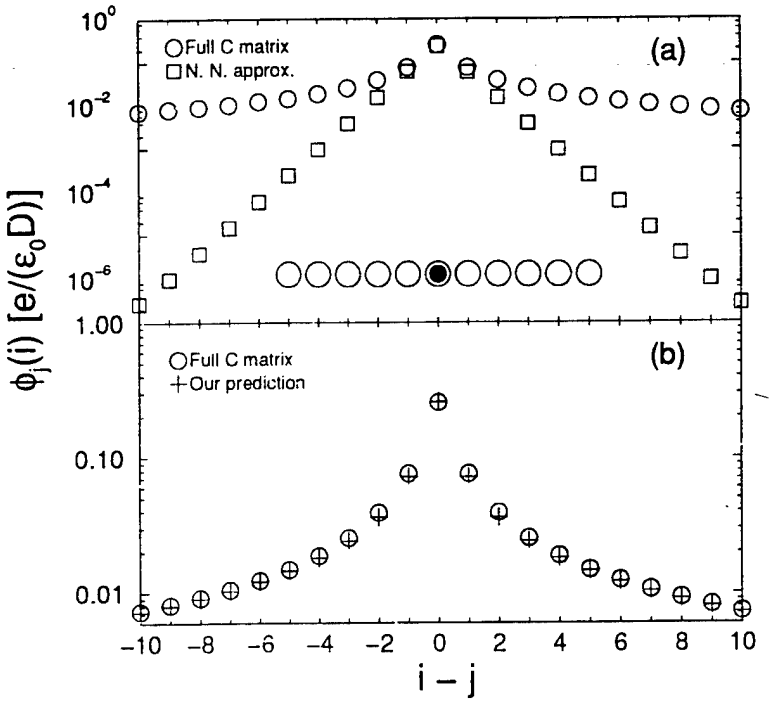

Figure 6: (a) The potential distribution due to a soliton located at the center ($i = 11$) of a 21×1 array. The circular symbol corresponds to the full capacitance matrix calculation and the square is for nearest neighbor approximation. The inset is a sketch of one section of our array. (b) The soliton potential distribution from the full capacitance matrix calculations (circles) compared to our predictions (crosses).

3 Numerical Simulations

We numerically calculated the full capacitance matrices for both one-dimensional (1D) and two-dimensional (2D) quantum-dot arrays. We found it necessary to use the full capacitance matrix in modeling coupled quantum dots due to weaker screening in these systems in comparison with arrays of normal metal tunnel junctions. The static soliton potential distributions in both 1D and 2D arrays are well approximated by the unscreened $(1/r)$ coulomb potential, instead of the exponential fall-off expected from the often-used nearest-neighbor approximation. In terms of dynamics, we compared the current-voltage (I-V) characteristics of voltage-biased 1D arrays using either the full capacitance matrix or its nearest neighbor approximation. The I-V curves show clear differences and the differences become more pronounced when larger arrays are considered.

For quantum dot arrays made by electrostatic confinement of two-dimensional electron gas (2DEG) in GaAs/AlGaAs heterostructures [5], the array forms a co-planar structure with all dots residing in the 2DEG plane. The co-planar capacitors are far less effective than parallel plates in terms of confining electric field. Therefore, in comparison with tunnel junctions, the field lines originating from one of those dots are much less confined and can reach out to dots that are much further apart. Hence, a model that only considers nearest neighbor capacitive coupling is unlikely to apply in this situation.

In our model, the quantum dots (small puddles of a 2DEG) are treated as thin circular shaped

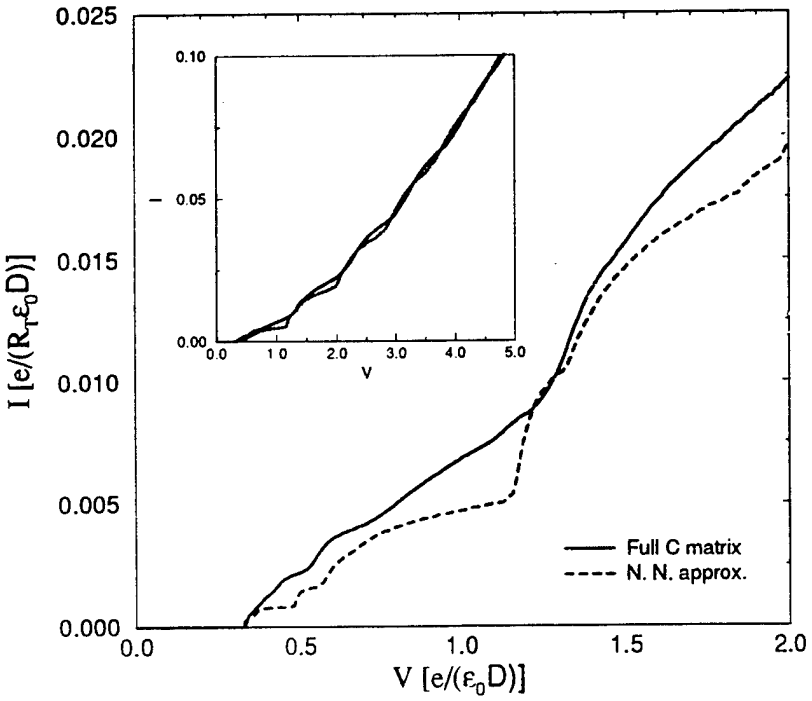

Figure 7: Current-voltage characteristics of a 21 × 1 quantum dot array using, the full capacitance matrix (solid line) and the nearest neighbor approximation (dashed line). The inset shows the I-V at a larger scale.

conducting plates. We take the diameter of the plates $D = 1\ \mu$m. The plates are arranged to form either 1D or 2D arrays with lattice constant $a = D + d = 1.1\ \mu m$, (assuming $d = 0.1\ \mu$m). Once the array geometry is specified, we compute the full capacitance matrix $\mathbf{C}$ of the 1D and 2D arrays using FASTCAP, an efficient capacitance extraction tool [6].

In Fig. 6a, we show the potential distribution due to a soliton being located at the center ($i = 11$) of a 21 × 1 series array, using both the full capacitance matrix and its nearest neighbor approximation. As we can see, the nearest neighbor approximation gives an exponentially decaying soliton potential as expected [7]. However, the soliton potential distribution that we get from the full capacitance matrix decays much slower. In Fig. 6b, we compare the full capacitance matrix soliton potential distribution with a simple Coulomb potential with a point charge e located at the soliton position (i.e. at the center of the 21 × 1 array). We see that the soliton potential follows the simple $1/r$ law almost exactly in the entire range, except at the origin where the Coulomb potential is singular.

We computed the current-voltage (I-V) characteristics of an array, which is typically what one measures in experiments. We compare, in Fig. 7, I-V curves for a 21 × 1 array computed using the full capacitance matrix and the nearest neighbor approximation. In computing these I-V curves, we use a Monte Carlo method [7–9]. As we can see in Fig. 7, the two I-V curves clearly show many differences. The threshold voltages are not exactly the same, and the fine structures are different and they become more pronounced if we consider larger arrays. At high voltage, the two curves merge and becomes nearly linear, as shown in the inset of Fig. 7. We see that the full capacitance matrix is necessary in the dynamical simulation of these arrays.

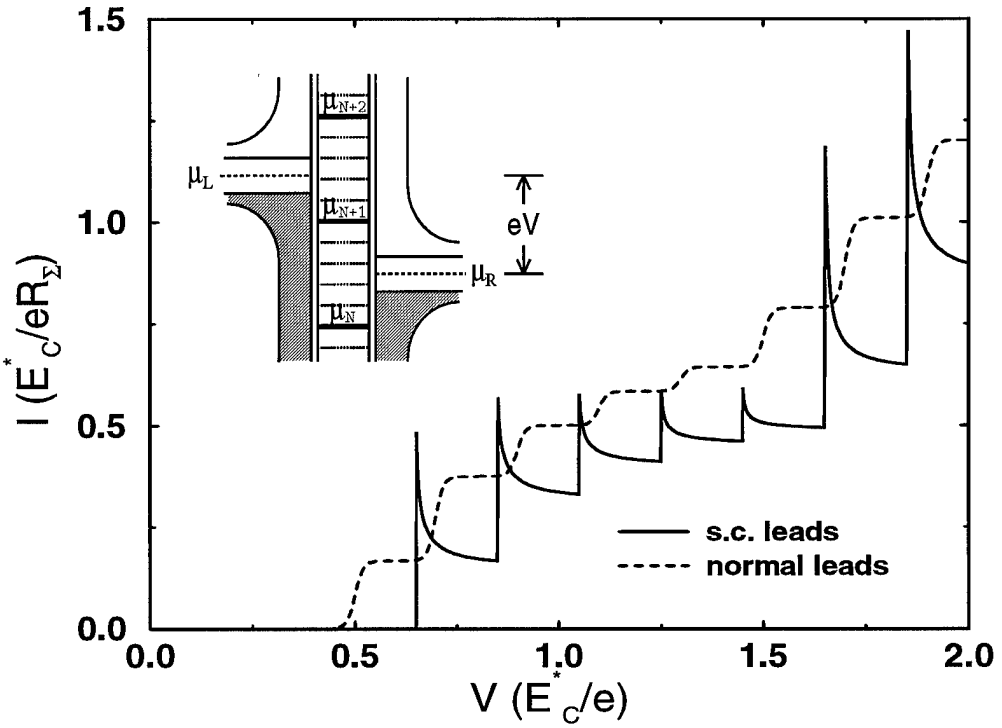

Figure 8: Low temperature I-V characteristics of a quantum dot with superconducting leads (solid curve) and normal metal leads (dashed curve). The temperature is $k_BT = 0.02E_C^*$, and the superconducting energy gap in the leads is $2\Delta = 0.3E_C^*$. The quantum level spacing is, $\epsilon = 0.2E_C^*$. The inset is a sketch of the energy spectra in the leads and the dot. Note the quantum dot energy spectrum includes the excitation spectrum (with spacing ϵ), and addition spectrum (with spacing $E_C^* = e^2/C + \epsilon$).

We also carried out numerical simulations of single-electron transport through a quantum dot with superconducting leads, based on the experimental system studied by Ralph *et al.* [10] To do this, we introduced a general phenomenological model of transport through a quantum dot. In this model, we assume that the quantum dot is weakly coupled to the two leads by tunnel barriers. When an appropriate bias voltage V is applied to the leads, an electron can tunnel across one barrier into the dot and subsequently tunnel out through the second barrier. According to general tunneling theory, the tunneling rate across a barrier from side "a" to side "b", can be evaluated using the Fermi's Golden Rule,

$$\Gamma_{a\to b}(\mu_a,\mu_b) = \frac{2\pi}{\hbar}\int_{-\infty}^{\infty} |T_{ab}|^2 \mathcal{N}_a(E-\mu_a)\mathcal{N}_b(E-\mu_b) f(E-\mu_a)\left[1-f(E-\mu_b)\right] dE, \qquad (1)$$

where T_{ab} is the phenomenological tunneling matrix element, and $f(x) = 1/[1+\exp(x/k_BT)]$ is the Fermi function. $\mathcal{N}_a(E)$ and $\mathcal{N}_b(E)$ are the density of states, and μ_a and μ_b are the chemical potentials, on their corresponding sides. For our system, to compute the tunneling rate from one of the leads to the dot, we take the BCS quasiparticle density of states in the lead and assume that the dot itself has an evenly spaced (with spacing ϵ) discrete level spectrum.

In Fig. 8, we show a typical low temperature current-voltage (I-V) characteristic of the system. Here the temperature $k_B T = 0.02 E_C^*$ ($E_C^* \equiv E_C + \epsilon$ is the spacing between chemical potential levels, and $E_C \equiv e^2/C_\Sigma$ is the charging energy), the superconducting energy gap $2\Delta = 0.3 E_C^*$ and the quantum energy level spacing in the dot $\epsilon = 0.2 E_C^*$. When the leads are superconducting (solid curve), the I-V curve consists of a series of sharp peaks spaced ϵ apart. This is in contrast with the I-V curve of the same dot with normal metal leads (dashed curve), which has only gentle steps with the same spacing ϵ. Fig. 8 is in good qualitative agreement with the experiment of Ref. [10].

In addition to the low temperature transport, our analysis shows that at higher temperatures thermal excitation of quasiparticles in the leads and thermal population of the excited quantum levels within the quantum dot should lead to interesting changes in the I-V curves. We also predict that when RF radiation is coupled to the system, the photon-assisted tunneling phenomena should manifest itself by producing extra periodic structures in the I-V curves, which might be useful in the millimeter wave detector/mixer applications.

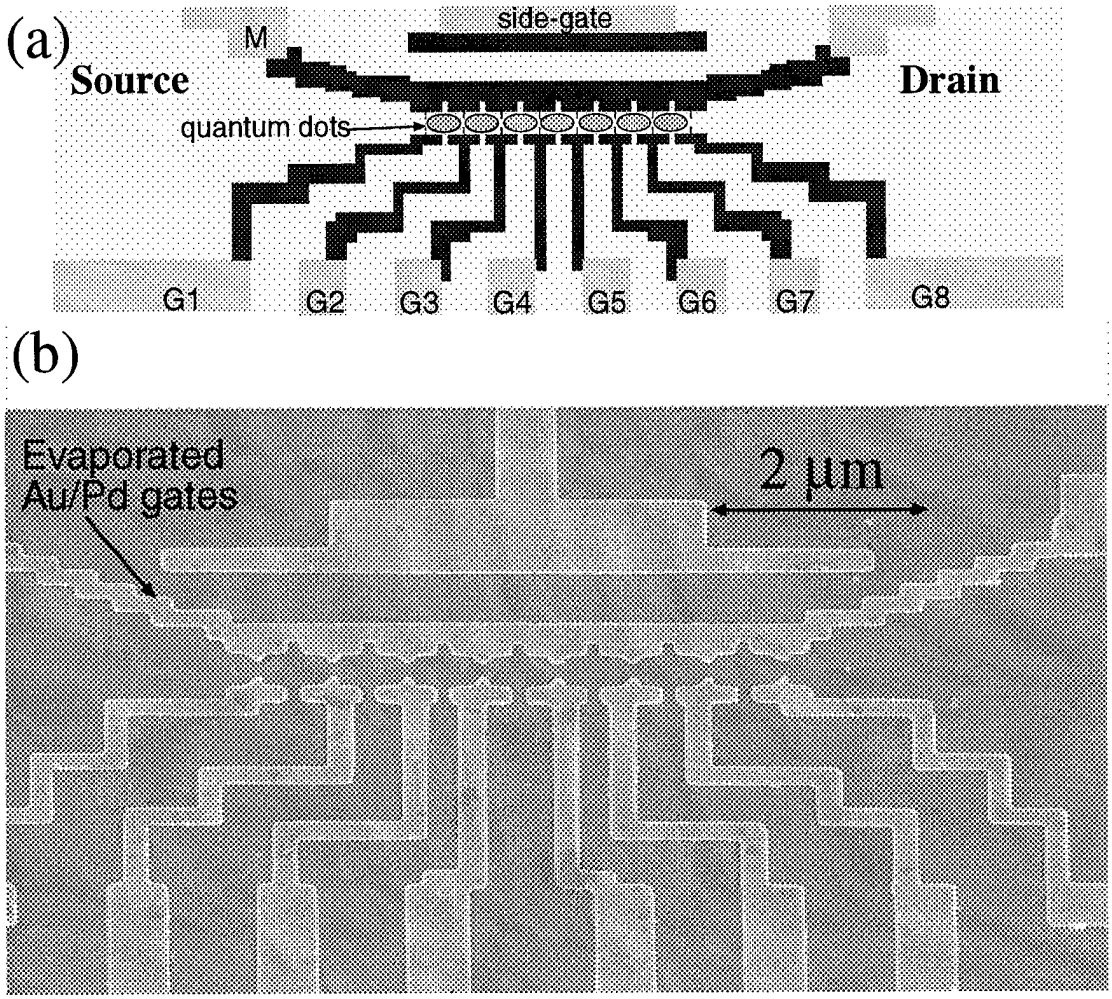

Figure 9: (a) Layout of a series array of seven quantum dots. The eight quantum point contacts are independently controlled to ensure array uniformity (b) SEM image of completed test device. The measured device has a smaller dot size – $500 \times 600\text{nm}^2$

4 Arrays of Quantum Dots

4.1 One-dimensional arrays

A one-dimensional array of seven quantum dots separated by eight quantum point contacts (QPCs) was fabricated by direct-write e-beam lithography on a GaAs/AlGaAs heterostructure. Figures 9(a) and 9(b) show respectively the device schematics and the SEM micrograph of a completed test device. The size of the dots in the measured device was $500 \times 600\text{nm}^2$.

Impurities in the semiconductor strongly affect the characteristics of the QPCs. For transport measurements is it essential that the tunneling conductance of each QPC in the array be the same. Therefore each QPC was controlled by a separate voltage source.

We performed low-temperature measurements of our device. First, we measured the total capacitance and various gate capacitances for a single dot in the array. The gate-to-dot capacitance is determined from the spacing between the Coulomb-blockade conductance peaks when the voltage on the gate is swept. The total capacitance of the dot can be determined in two ways. First, the total

dot capacitance can be found by analyzing a temperature dependence of the peak width. Second, it is given by the width of the Coulomb blockade region in the current-voltage (I-V) measurement. We have tried both techniques and obtained consistent results.

After verifying that the quantum dots had reasonable values for their capacitances, we repeated the double dot experiment first reported by Waugh *et al* [5]. The schematics of the experiments are shown in Fig. 10(a) A double quantum dot was created by applying appropriate voltages to gates M, G_5, G_6, G_7. The side-gate was then swept and Coulomb blockade oscillations were observed. Figure 10(b) shows changes in the pattern of Coulomb blockade oscillations with increasing inter-dot coupling. The voltage on G_6 was increased by 20 mV for each subsequent curve increasing conductance through QPC6 and thus increasing inter-dot coupling. We see that for a bottom curve the period of oscillations is 24 mV (corresponding to $C_{sg} = 7$ aF). Thus, for a system of two identical quantum dots we observe the regular peak period equal to the peak period of a single dot. On the next several curves each peak is split into two peaks which move farther apart as the interdot coupling increases. Finally, on the top curve we again see regular Coulomb blockade peaks, but with a different period – 9 mV (corresponding to $C_{sg} = 18$ aF). For this curve, the two original dots merged into one large dot which has approximately twice the capacitance to the gate and hence approximately half the oscillation period.

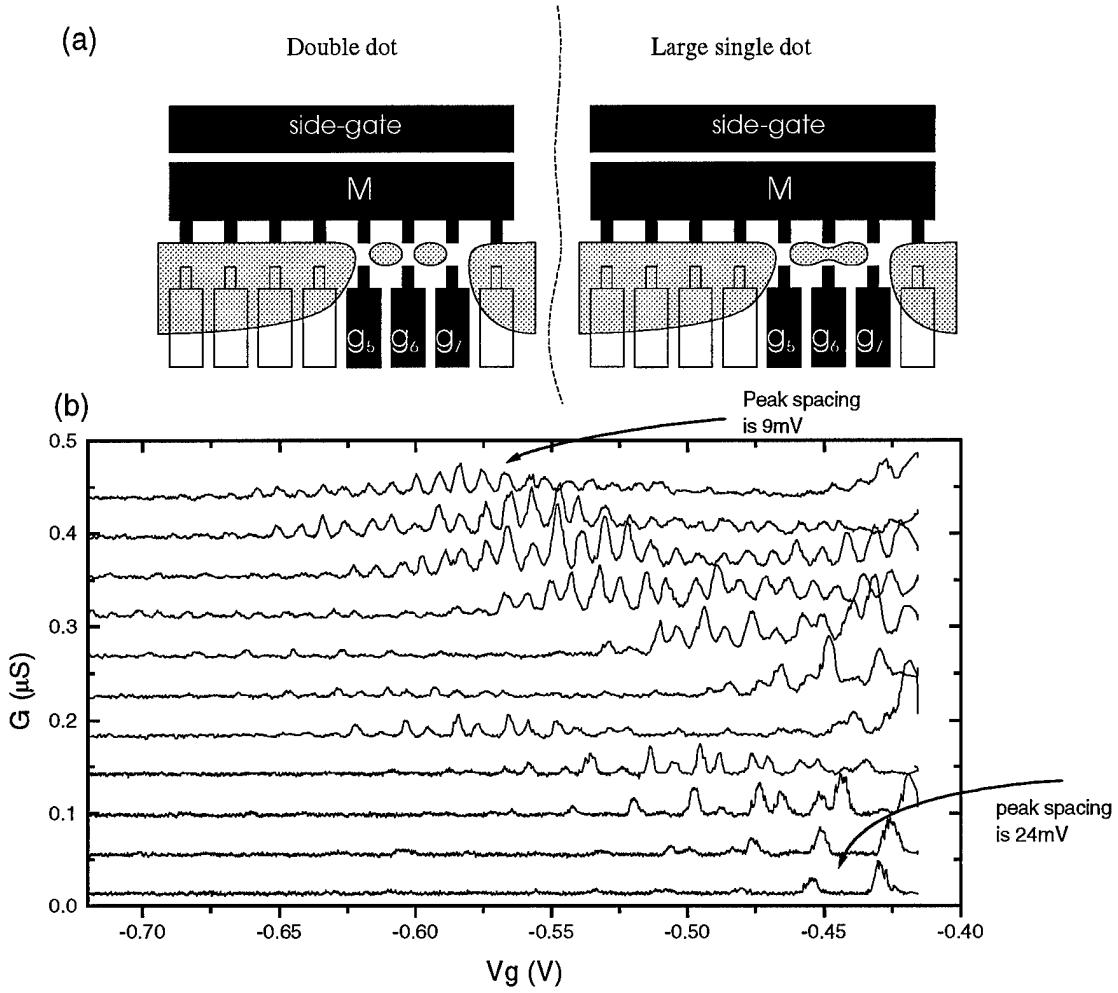

Figure 10: (a) Schematics of double dot experiment. By applying appropriate voltages to gates M,G_5 , G_6, and G_7 we can create either a double dot or single large dot depending of the voltage on G_6. (b) Experimental results. On the bottom curve QPC G_6 is closed, so we have a double dot. As the conductance of QPC G_6 is increased for each subsequent curve each peak is split into two. When QPC G_6 is open enough so that we have a single dot, the peak spacing becomes approximately half that for the double dot.

4.2 Two-dimensional arrays

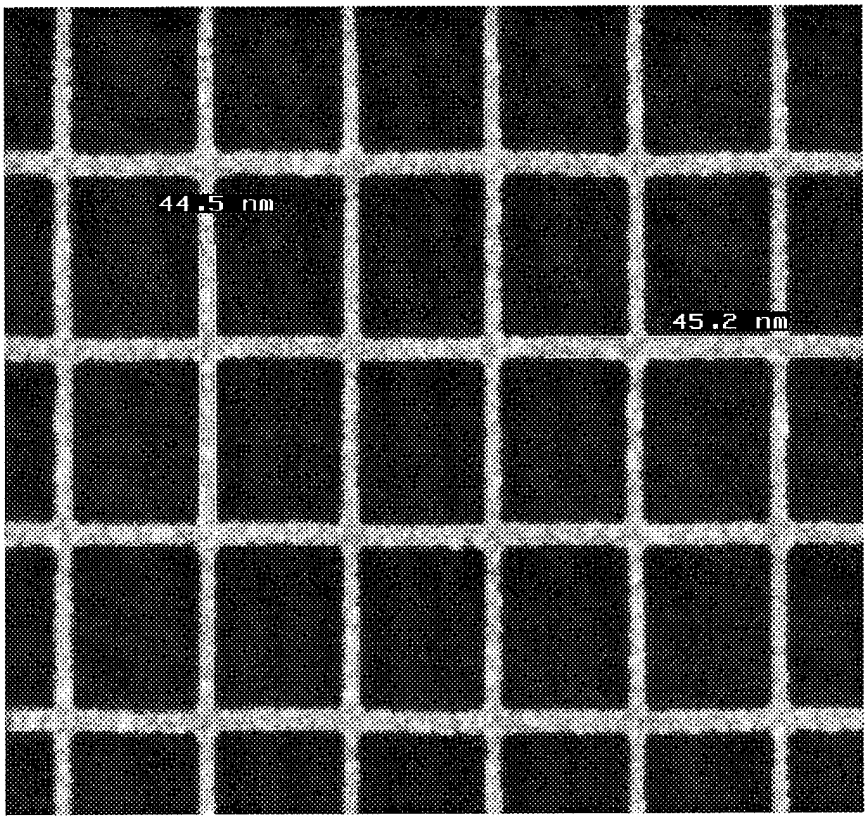

Figure 11: SEM micrograph of a 400 nm-period and 45 nm-linewidth Au grid gate on a 1μm thick silicon nitride membrane. The pattern was created by e-beam nanolithographjy and subsequent electroplating of 200nm thick Au.

We also investigated two-dimensional systems of quantum dots with controllable coupling between dots. This device is similar to a conventional high-electron-mobility transistors, but the gate is a metallic grid of fine period (150 – 400 nm), rather than the conventional continuous gate. Electrons under this gate see a periodic potential which is tunable by controlling the gate bias. The imposed periodic potential creates minibands superimposed on the band structure created by the crystalline periodic potential. In earlier research we observed electron back diffraction in 200 nm period, 65 nm-linewidth grid-gate structures. Additionally, negative differential conductance (NDC) was measured in devices with high source-to-drain bias applied [11, 12]. The NDC effect was attributed to sequential-resonant tunneling.

As was discussed in Section 2, production of devices with dimensions under 50 nm is challenging. The modifications to the x-ray mask process detailed in that section, however, allowed us to fabricate the necessary gate structures. Figure 11 shows a scanning electron micrograph of an x-ray "mother" mask which was used to do so.

5 Publications and Talks

5.1 Papers

1. C.B. Whan, J. White and T. P. Orlando, *"Full Capacitance Matrix of Coupled Quantum-Dot Arrays: Static and Dynamical Effects"*, Appl. Phys. Lett.,**68**, 2996 (1996).

2. C.B. Whan and T. P. Orlando, *"Transport properties of a quantum dot with superconducting leads,"* Phys. Rev. B (*Rapid Comm.*), **54**, R 5255 (1996).

3. C.B. Whan, *"Hierarchical clustering of energy levels in two-dimensional harmonic oscillators,"* Phys. Rev. E (*Rapid Comm.*), **55**(4), R3813–3816, (1997).

4. D.J.D. Carter, A. Pèpin, M.R. Schweizer, H.I. Smith, and L.E. Ocola, *"Direct Measurement of the Effect of Substrate Photoelectrons in X-ray Nanolithography"*, J. Vac. Sci. Technol. B, **15**(6), 2509–2513 (1997).

5.2 Talks

1. D.J.D. Carter, *"X-ray Nanolithography: Issues and Technology"*, Gordon McKay Laboratory, Harvard University, Cambridge, MA, September 15, 1995.

2. C.B. Whan, *"Quantum Dot Arrays: Concepts, Physics, and Possible Applications"*, Physics Department Colloquium, University of Massachusetts – Dartmouth, December 2, 1995.

3. A. Pèpin, *"Fabrication of lateral superlattices in GaAs/AlGaAs grid-gated MODFETs by X-ray nanolithography,"* Seminar, Physics Department, Boston College, Chestnut Hill, MA February 14, 1996.

4. C.B. Whan, *"Full Capacitance Matrix of Quantum Dot Arrays: Static and Dynamical Effects"*, March Meeting of the American Physical Society, St. Louis, Missouri, March 20, 1996.

5. C.B. Whan, *"Array of quantum dots: statics and dynamics"*, CSR Seminar, Center for Superconductivity Research, University of Maryland, April 23, 1996.

6. C.B. Whan, *"Full Capacitance Matrix of Quantum Dot Arrays: Static and Dynamical Effects"*, NATO Advanced Study Institute on "Mesoscopic Electron Transport", Curacao, June 25, 1996.

7. C.B. Whan, *"Single electron tunneling through a quantum dot with superconducting leads"*, NATO Advanced Study Institute on "Mesoscopic Electron Transport", Curacao, June 25, 1996.

8. Mark Schweizer, Ilia Sokolinski and Henry I. Smith, *"Research in the NanoStructures Laboratory at MIT"*, Gordon Research Conference on the Chemistry and Physics of Nanostructure Fabrication, New England College, Henniker, New Hampshire, June 25, 1996.

9. C.B. Whan, *"Single electron transport in semiconductor quantum dot devices"*, Wolfgang Kroll Memorial Symposium, University of Massachusetts - Dartmouth, North Dartmouth, Massachusetts, August 16, 1996.

10. D. Antoniadis, D. Berman, D. Carter, K. Jackson, M. Meinhold, T. Orlando, A. Pepin, M. Schweizer, H. Smith, I. Sokolinski, I. Yang, *"Nanostructured Electronic and Quantum-effect Devices"*, Research Laboratoy of Electronics 50th Anniversary, Massachusetts Institute of Technology, Cambridge, Massachusetts, November 1, 1996.

11. D. Berman, D. Carter, K. Jackson, M. Meinhold, A. Pepin, M. Schweizer, I. Sokolinski, I. Yang, D. Antoniadis, T. Orlando, H. Smith, *"Nanostructured Electronic and Quantum-effect Devices"*, Microsystems Technology Laboratories Annual Review, Massachusetts Institute of Technology, Cambridge, Massachusetts, January 17, 1997.

References

[1] H. I. Smith and D. A. Antoniadis. Seeking a radically new electronics. *Technology Review*, 93:26, April 1990.

[2] Michael Biafore. *Few-Body Cellular Automata: A Method for Extracting Useful Computation from Physical Interactions.* PhD thesis, Massachusetts Institute of Technology, December 1993.

[3] C. S. Lent, P. D. Tougaw, and G. H. Bernstein. Quantum cellular automata. *Nanotechnology*, 4:49, 1993.

[4] W. Warren. The usefullness of quantum computing. *Science*, 277:1688–1689, 1997.

[5] F. R. Waugh, M. J. Berry, D. J. Mar, R. M. Westervelt, K. C. Campman, and A. C. Gossard. Single-electron charging in double and triple quantum dots with tuneable coupling. *Phys. Rev. Lett.*, 75(4):705–708, July 1995.

[6] K. Nabors, S. Kim, and J. White. Fast capacitance extraction of general three-dimensional structures. *IEEE Trans. on Microwave Theory and Techniques*, 40(7):1496–1507, July 1992.

[7] N. S. Bakhvalov, G. S. Kazacha, K. K. Likharev, and S. I. Serdyukova. Single-electron solitons in one-dimensional tunnel structures. *Zh. Eksp. Theor. Fiz.*, 95(3):1010–1021, 1989. [*Sov. Phys. JETP* 68, 581(1989)].

[8] N. S. Bakhvalov, G. S. Kazacha, K. K. Likharev, and S. I. Serdyukova. Statics and dynamics of single-electron solitons in two-dimensional arrays of ultrasmall tunnel junctions. *Physica B*, 173(3):319–328, 1991.

[9] U. Geigenmüller and G. Schön. Single-electron effects in arrays of normal tunnel junctions. *Europhys. Lett.*, 10(8):765–770, 1989.

[10] D. C. Ralph, C. T. Black, and M. Tinkham. Spectroscopy of the superconducting gap in individual nanometer-scale aluminum particles. *Phys. Rev. Lett.*, 54:3241, 1995.

[11] Khalid Ismail. *The Study of Electron Transport in Field-Effect-Induced Quantum wells on GaAs/GaAlAs.* PhD thesis, Massachusetts Institute of Technology, May 1989.

[12] K. Ismail, W. Chu, A. Yen, D. A. Antoniadis, and Henry I. Smith. Negative transconductance and negative differential resistance in a grid-gate modulation-doped field-effect transistor. *Appl. Phys. Lett.*, 54(5):460–462, January 1989.